A&A 423, 391–395 (2004)
DOI: 10.1051/0004-6361:20034532

Astronomy & Astrophysics

Modelling the Lyman β dayglow in the Jovian atmosphere⋆

M. Barthélemy[1], C. Parkinson[2,3], J. Lilensten[1], and R. Prangé[4]

[1] Laboratoire de Planétologie de Grenoble, CNRS-UJF, BP 53, 38041 Saint Martin d'Hères, Cedex 9, France
e-mail: mathieu.barthelemy@ujf-grenoble.fr
[2] MS 150-21, Caltech, Pasadena, California 91125, USA
[3] MS 183-501, JPL, Pasadena, California 9110, USA
e-mail: cdp@gps.caltech.edu
[4] Observatoire de Paris-Meudon, 5 place Jules Jansen, 92195 Meudon, France
e-mail: renee.prange@obspm.fr

Received 17 October 2003 / Accepted 15 March 2004

Abstract. The Lyman β dayglow of Jupiter provides an important source of information about its atmosphere. The H Lyman β and the $H_2$6–0 P(1) line of the Lyman system overlap, resulting in a coupling effect between these two lines. In this paper, we evaluate the effect of this overlapping via radiative transfer modelling and show its effect both on the integrated intensity and the line profile. The intensity increases at about 1025 Å at the centre of the disc, tends to slightly decrease at the limb, and creates an asymmetry in the profile. This asymmetry is also present in the jovian H-Lyman α bulge region.

Key words. radiative transfer – planets and satellites: individual: Jupiter – ultraviolet: solar system

1. Introduction

Studying the H-Lyman α dayglow for the giant planets is very useful in obtaining information about their atmospheres. Several previous studies have been done on the Lyman α dayglow (Wallace & Hunten 1973; Yung & Stroebel 1980; Shemansky 1985; Ben Jaffel et al. 1988; Emerich et al. 1993; Griffioen 2000), but the Lyman β problem has been virtually unstudied for Jupiter. One reason for this is that the H Lyman lines are close to some lines of the H_2 Lyman system, i.e. electronic transition between the ground state $X^1\Sigma_g^+$ and the excited state $B^1\Sigma_g^+$. For instance, the wavelength difference between the H_2(6−0 P(1)) and the H-Lyman β lines is 0.21 Å. This coincidence cannot be neglected in the atmosphere of the giant planets because of the presence of both molecular and atomic hydrogen in comparable quantities.

Previously, the Jovian Lyman β problem has only been modelled as a single independent line (Gladstone 1988) using a Feautrier radiative transfer technique. This study focuses on two atomic oxygen lines for Earth and the Lyman α and β lines for Jupiter. An intensity of 10 R was predicted for the Lyman β line at the centre of the disk with the viewing angle of 20° with respect to the overhead sun. It was also seen that Lyman β is limb-brightened due to the increased H column along the line of sight at the limb.

There have been other approaches to this problem. For instance, Feldman et al. (1993) analysed the HUT (Hopkins University Telescope) data, but its resolution of about 3 Å does not give direct information on the line profile. Using a solar flux of $6 \times 10^{+9}$ ph cm^{-2} s^{-1} at 1 AU, the authors found a total emission of 30 ± 7 R at 1025 Å. The total emission consisted of two components: 10−12 R from the H_2 6−0 P(1) emission and 18−20 R from the Lyman β emission. The contribution of the H_2 line was calculated by an analysis of the fluorescence spectra emitted by Jupiter on the Lyman system. They have also estimated that the total fluorescence on the Lyman system due to solar Lyman β line is 100 R.

Liu & Dalgarno (1996) addressed the same problem but including coupling between these two lines. They calculated the fluorescence on all molecular hydrogen lines due to the pumping of H Lyman β and found that 59% of the total solar Lyman β line is pumped. No information is given about the line profile. They obtain 17.5 R for the solar Lyman β resonance scattering and 10.4 R for the H_2 6−0 P(1) line for a solar flux of about $8 \times 10^{+9}$ ph cm^{-2} s^{-1} at 1 AU.

In this study, we use a radiative transfer approach to address the computation of the dayside Jovian H Lyman β emission taking into account the coupling with the molecular hydrogen lines. From this approach we obtain both the intensity and the line profile shape.

2. Model

Our radiative transfer method follows the Feautrier approach used by Gladstone (1983, 1988). Griffioen (2000) and Parkinson (2002) extended this model to include the case of

⋆ Appendix A is only available in electronic form at http://www.edpsciences.org

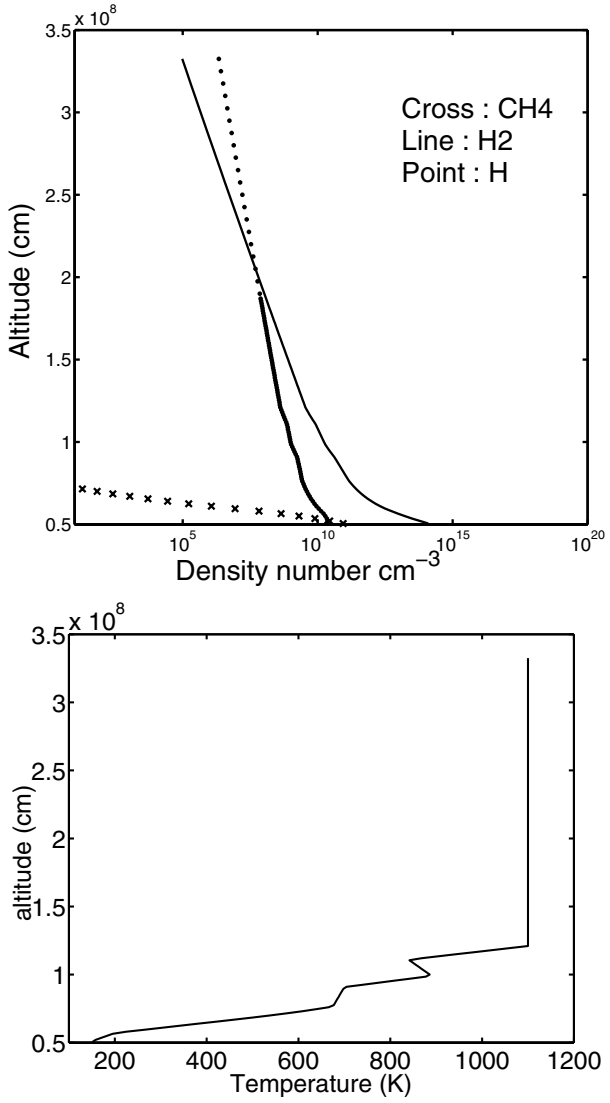

Fig. 1. Jovian neutral atmosphere, *top panel*: composition, *bottom panel*: temperature (non-bulge region).

coupled H and D Lyman α (see Appendix A for details). Their coupled case used a rapidly convergent lambda operator method for solving the resonance line scattering problems (cf. Griffioen et al. 1994) which we employ here. We found that a calculation using this improved method with 112 altitude levels, more than 100 frequencies and 16 angles took only ~4 min to run, compared to 8 h using an adding doubling method! The Feautrier technique allows us to keep information about the emission for each altitude level and allows the sphericity of the planet to be taken into consideration for precise limb computations.

2.1. Neutral atmosphere

We use H, H_2 and CH_4 profiles taken from Parkinson (2002) as shown in Fig. 1, corresponding to solar minimum conditions. The Eddy diffusion coefficient at the homopause, K_h, is 2×10^6 cm^2 s^{-1} (Vervack et al. 1995).

Table 1. Spectroscopic parameters for H Lyman β and H_2 P(1) 6−0 lines.

Line	λ(Å)	g_1	g_2	f	$A(10^8\ s^{-1})$	ϖ
H Ly β	1025.72	2	6	0.0791	1.672	0.8816
H_2 line	1025.93	3×3	1	0.00912	1.7	0.1357

At lower thermospheric altitudes (between 500 km and 2000 km above the 1 bar level), molecular hydrogen is the main species. For higher altitudes, atomic hydrogen becomes more abundant because of H_2 photodissociation. As CH_4 is the prime Lyman series absorber, it cannot be neglected above the $\tau_{CH4} = 1$ level located at approximately 500 km. The exospheric temperature is obtained from the Galileo probe measurements (Seiff et al. 1997) and is ~1100 K.

2.2. Solar flux

The input solar flux is modelled by a double Gaussian profile (Lemaire 1978; Gladstone 1988) given by

$$\pi F(x) = \frac{\pi F}{2x_0\sqrt{\pi}} \left\{ \exp\left[-\left(\frac{x - x_1}{x_0} \right)^2 \right] + \exp\left[-\left(\frac{x + x_1}{x_0} \right)^2 \right] \right\} \quad (1)$$

where $x_1$is the offset for each peak from the line centre, and x_0 is the width for each Gaussian function. The Lyman β line centre wavelength is 1025.72 Å and we take $x_0 = 12.5$ sdu (standard doppler units) and $x_1 = 14.6$ sdu (Gladstone 1988). For this line 1 sdu = 9.8 mÅ at a reference temperature of 500 K. For solar minimum conditions, $\pi F = 4.0 \times 10^9$ ph cm^{-2} s^{-1} at 1 AU.

2.3. Spectroscopic parameters

The H Lyman β line parameters are taken from Gladstone (1988) and the molecular hydrogen line parameters are from Abgrall et al. (1993). However, we must calculate for each line the single scattering albedo ϖ defined by:

$$\varpi = \frac{A_{ij}}{\sum_k A_{kj}}$$

where i is the lower level, j the upper level, and k is all the levels with allowed transitions starting from j. We consider that the Lyman system is isolated, and so we only consider rovibronic transitions: that is to say, all the vibrational (v) and rotational (J) levels with selection rules $\Delta J = \pm 1$.

$\Delta J = 0$ is a forbidden transition, as for both electronic states of the Lyman system the electronic quantum number is 0. There is no rule for vibronic transitions.

The spectroscopic parameters for H Lyman β and H_2 P(1) 6−0 are given in Table 1.

We can now compute the H_2 populations in each vibrational and rotational level starting from the total density N_0 and considering 15 rotational levels for each vibrational level. We only consider the first two vibrational levels since the higher vibrational levels are so high that their populations are negligible by

comparison. The energy levels come from Abgrall et al. (1993) and their populations are given by:

$$N(vJ,z) = N_0(z)\,\frac{(2J+1)\,g_s \exp(-E_{vJ}/kT)}{\sum_{vJ}(2J+1)\,g_s \exp(-E_{vJ}/kT)} \quad (2)$$

where:

E_{vJ} is the energy of the level with vibrational number v and rotational level J;

g_s is the spin degeneracy and is equal to 3 for odd rotational level and to 1 for the others.

To take into account frequency redistribution, we use the angle-averaged partial redistribution function $r(z, \mu, x, \mu', x')$ given by Hummer (1962) and Mihalas (1978). We assume that σ_{CH4} is independent of the frequency and that its value is 3.2×10^{-17} cm^2 at 1025 Å (Berkowitz 1979).

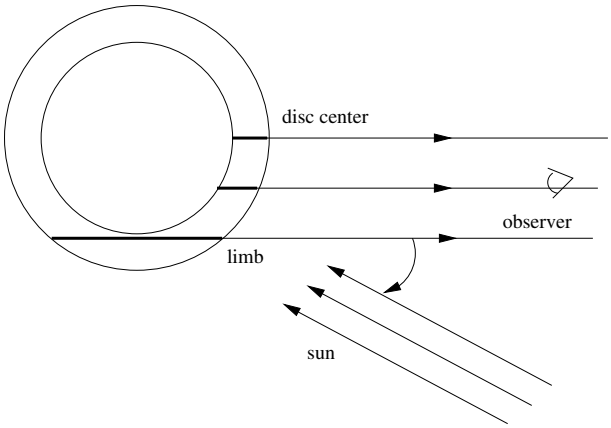

Fig. 2. Jupiter/Sun/observer geometry. Bold lines represent the path of lines of sight through the atmosphere at the centre of the disk and at the limb.

3. Results

3.1. Integrated brightness

We validate our results by studying the uncoupled case and obtain a Lyman β intensity of 20.63 R at the disk centre. This is slightly larger than previous studies: 18 to 20 R measured by the HUT telescope by Feldman et al. (1993) and 17.5 by Liu & Dalgarno (1996) with a different modelling method for H Lyman β only. With comparable solar input fluxes, our results in the uncoupled case gives 30.94 R in Feldman et al. (1993) conditions and 41.26 R in Liu & Dalgarno conditions. If we consider the global intensity for both lines, our value is comparable to the value (30 ± 7 R) measured by Feldman et al. (1993) but it is more than the value calculated by Liu & Dalgarno (1996).

At the limb, we obtain an integrated intensity of 49.6 R. This can only be compared to the theoretical Gladstone (1988) value of 25 R as there are no data available. The large discrepancy observed is mainly due to the atmospheric model as our H column density is about ten times larger.

We now consider the coupled line case. In the non-bulge region, we obtain a line-integrated intensity of 23 R at the disk centre with a solar zenith angle of 20°. This is 10.3% larger than for the uncoupled case. At the limb, with a point of sight at 1.008 Jovian radius we obtain 48.1 R with an angle of 20° between the viewing angle and the sun direction. This value is smaller than for the uncoupled case by 3%. Figure 2 shows that this result is due to a geometric effect. At high altitude, the atmospheric molecular hydrogen in the atmosphere is excited by an intense solar Lyman β line that is scattered in all directions, including toward the observer. There is slight H Lyman β self absorption because this line is not conservative but there is a strong absorption due to fluorescence of the 6–0 P(1) line on other lines of the Lyman system. Part of the H_2 absorption is emitted in other wavelengths and then lost for the coupling with H-Lyman β. Further down in the atmosphere, the molecular hydrogen becomes more important and absorbs more solar photons. A photon emitted by H_2 at low altitude will have a larger probability to be absorbed by H_2 before it can leave the atmosphere. After 4 scatters by H_2, the probability that a photon has disappeared is 0.99966.

Therefore, the larger the atmospheric slab, the larger the frequency redistribution of the photons toward wavelengths outside the H-Lyman β region, and it is normal that, at the limb, we obtain a smaller brightness for the coupled case than for the uncoupled case.

3.2. Spectral line profile

Figure 3 shows the effect of the H–H_2 coupling on the line profile. The presence of H_2 has a strong effect on the line profile, especially at the limb. On the red side of the line we can see the peak due to the H_2 line emissions at $\lambda \sim 0.2$ Å. However, the most interesting feature is the asymmetry of the two wings of the H-Lyman β line at the limb when coupling is taken into account. Due to the already discussed geometrical effect, the red side of the Lyman β line is pumped by the absorption of the H_2 molecule. We can explain this phenomenon as follows. At the limb, the line of sight passes through a very thick layer of atmosphere, greatly increasing the effects of the absorption for this case. We can identify redistribution effects at the limb around the central peak as calculated and discussed by Gladstone (1988). These effects are assigned to frequency redistribution effects of H atoms. This last effect is mainly due to the large H column density at the limb. This phenomenon is characteristic of the radiative transfer for non-conservative lines with an angle-averaged redistribution function (Gladstone 1988).

At the centre of the disk, the strong asymmetry is not present because the H_2 self-absorption does not play any role. We note that the red side of the line is slightly higher than the blue side. Following Gladstone (1988), we cannot identify any redistribution effect at the centre of the disk. At $\lambda \sim 0.2$ Å, we still see the H_2 emission peak. This peak is only due to the upper layers of the atmosphere because of the strong H_2 self-absorption.

For both cases, we see that, unlike the red wing, the intensity and the shape of the line centre are not affected by the overlapping. This is due to the partial redistribution function used in our calculation, which assumes little interaction between the centre of the line and the wings.

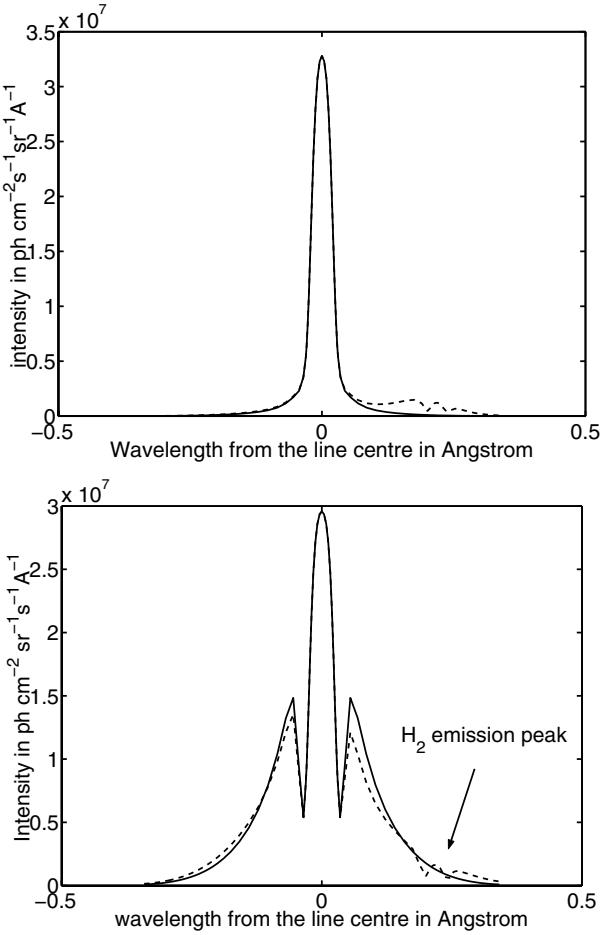

Fig. 3. Line profiles. The upper panel is for the centre of disc case. The other panel is at the limb. Solid lines: the uncoupled case, dashed lines: coupled case.

3.3. Centre-to-limb variations

The centre-to-limb variation is shown in Fig. 4: on the disk, the shape is as before but the uncoupled case has a lower intensity. At the limb the peak is quite similar for both the uncoupled and coupled cases, comparing favourably with previous results (Gladstone 1988). On the entire disk (impact parameter less than 1) the brightness in the coupled case is greater than in the uncoupled case.

3.4. H_2 self-absorption contribution

The brightness of the emission computed here for H_2, in the coupled case, is smaller than in the measurements of Feldman et al. (1993) using the HUT telescope (Feldman 1993) or that predicted by Liu & Dalgarno (1996) without radiative transfer. Both authors found an intensity of 10 to 12 *R* for the contribution of the H_2 lines, which were averaged over the entire disk. Because of the coupling, it is difficult to estimate the contribution of H and H_2. We can only say that the difference between the uncoupled and coupled cases has a maximum of 2.4 *R*. So the upper value to the H_2 contribution is 2.4 *R* at the disk centre. This discrepancy can be attributed to the H_2 self-absorption. In previous studies, it has been shown than the Lyman β emission

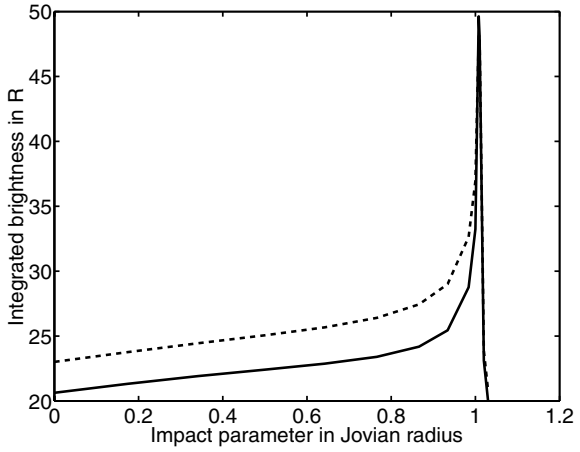

Fig. 4. Jovian H Lyman β centre-to-limb variation. Solid line: uncoupled case, Dashed line: coupled case.

is larger than the H_2 6−0 P(1) emission. This is the case also in the present work, but the ratio is found to be still larger than in previous works.

To understand the role of the H_2 self-absorption, we compare the previous calculation to a new calculation with a single scattering albedo $\varpi_{H2} = 1$. It will give the possibility to estimate the brightness lost by the H_2 self absorption. In this case, we find an intensity of 90.7 *R* at the centre of the disk and 131.5 *R* at the limb. The line profile shows a very strong peak due to the H_2 line and the Lyman β contribution is not changed. Hence, we can estimate the difference between this case and the physical case that the effect of the self-absorption caused by the H_2 line on the total integrated brightness is around 70 *R* at the centre of the disk and 84 *R* at the limb. If we consider an input solar flux of 8k *R* at 1 AU, we obtain 140 *R*, i.e. less than the 175 *R* calculated by Liu & Dalgarno (1996). For comparison to the results of Feldman et al. (1993), we consider now a solar input flux of 6 kR at 1 AU In this case, our value becomes 105 *R*, which is close to their value (100 *R*).

3.5. Lyman α bulge region

Another interesting effect takes place in the Jovian bulge region. This bulge was first observed in 1978 by a sounding rocket (Clarke et al. 1980) and confirmed by the Voyager observations in 1979 (Sandel et al. 1980), which showed a strong excess in the Lyman α emission centred on the magnetic drift equator latitude, and fixed in magnetic longitude (system III) at $\lambda_{III} = 100°$. Sommeria et al. (1995) suggested that it could be due to strong jets in the upper atmosphere, explaining the strong heating observed in this region, where the temperature increases drastically between 2000 km and 2500 km to more than 6000 K (see Fig. 5). This high temperature implies changes in the absorption and scattering cross sections and in the width in the line profiles.

We have calculated the Lyman β line profile in the bulge region (see Fig. 6). Our simulation shows a very strong frequency redistribution effect on photons near the central frequency due to this hot layer. This absorption effect is so strong that for some frequencies the emergent intensity is equal to zero. In contrast

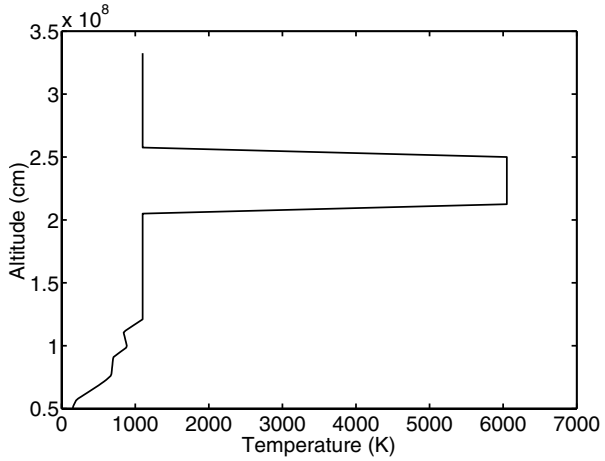

Fig. 5. Atmospheric temperature profile in the bulge region (Parkinson 2001).

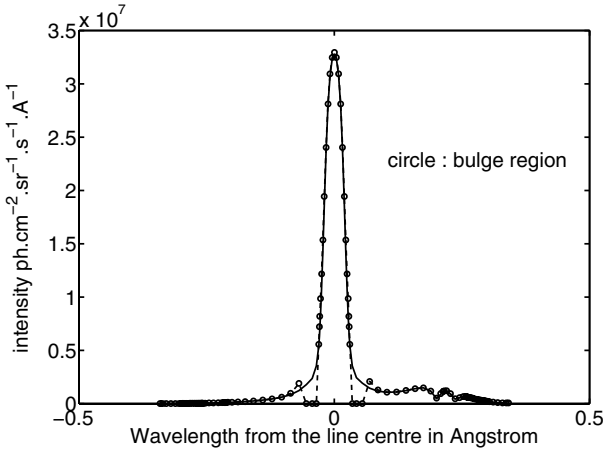

Fig. 6. Jovian Lyman β line profiles. The dashed line drawn through the circles correspond to the bulge region. The solid line is for the non-bulge region.

with the other regions, in the bulge this reversal is present even at the centre of the disk, for short optical paths.

At the centre of the disk, the Lyman β brightness equals 22 *R*. It is smaller than in the non-bulge region. It reveals that we find no increase of the Lyman β bulge intensity because of the self-absorption of the line.

This means that this layer increases the optical depth and the effect of the frequency redistribution close to the central peak. However, the effects of the bulge on the coupling are not very different than in non-bulge regions.

4. Summary

In this paper, we have studied the influence of the coupling between the H Lyman β line at 1025.72 Å and the $H_2$6−0 P(1) line of the Lyman system on the emission reflected by the Jovian atmosphere. We have used a radiative transfer code resolving the radiative transfer equation by a Feautrier method, with an angle-averaged redistribution function.

As expected, and in agreement with Gladstone (1983), we obtain Lyman β line profiles which vary from peaked lines to self reversed lines as the line of sight crosses thin (disk centre) to thick atomic H layers.

We then find that the effect due to the H and H_2 line overlapping is significant, affecting both the line-integrated brightness and the line profile. These effects increase the intensity around 1025.7 Å ± 0.3 Å for emission from the disk centre (20.63 *R* versus 20.03 *R*), but the overlapping tends to slightly decrease it at the limb (49.6 *R* versus 48.1 *R*). In addition, the line-coupling creates an asymmetry on the profile due to the self-absorption of H_2.

In future work, we hope to check our results against measurements made by FUSE (Far Ultraviolet Spectroscopic Explorer) of the EUV emissions from Jupiter. Its high spectral resolution (~0.05 Å) and its spectral band between 900 Å and 1200 Å, makes this instrument the most relevant for the Lyman β line.

References

Abgrall, H., Roueff, E., Launay, F., Roncin, J. Y., & Subtil, J. L. 1993, A&AS, 101, 273
Ben Jaffel, L., Magnan, C., & Vidal-Majar, A. 1988, A&A, 204, 319
Berkowitz, J. 1979, Photoabsorption, photoionization and photoelectron Spectroscopy (Academic Press)
Cannon, C. J. 1985, The transfer of spectral line radiation (Cambridge University Press)
Clarke, J. T., Weaver, H. A., Feldman, P. D., et al. 1980, ApJ, 240, 696, Part 1
Emerich, C., Ben Jaffel, L., & Prangé, R. 1993, 41, 363
Feldman, P. D., McGrath, M. A., Moos, H. W., et al. 1993, ApJ, 406, 279
Gladstone, G., & Randall 1983, Ph.D. Thesis, California Inst. of Tech., Pasadena
Gladstone, G., & Randall 1988, JGR, 93, 14623
Griffioen, E., McConnell, J. C., & Shepherd, G. G. 1994, JGR, 99, 21, 383
Griffioen, E. 2000, JGR, 105, E10, 24613
Hummer, D. G. 1962, MNRAS, 125, 21
Lemaire, P., Charra, J., Jouchoux, A., et al. 1978, ApJ, 223, L55
Liu, W., & Dalgarno, A. 1996, ApJ, 467, 446
Mihalas, D. 1978, Stellar atmospheres, 2nd edition, W. H. Freeman and Co.
Parkinson, C. D. 2002, Ph.D. Thesis, York University, North York, Ontario
Sandel, B. R., Broadfoot, A. L., & Strobel, D. F. 1980, GRL, 7, 5
Seiff, A., Kirk, D. B., Knight, T. C. D., et al. 1997, Science, 276, 102
Shemansky, D. E. 1985, JGR, 90, 2673
Sommeria, J., Ben Jaffel, L., & Prangé, R. 1995, Icarus, 118, 2
Vervack, R. J., Jr, Sandel, B. R., Gladstone, G., et al. 1995, Icarus, 114, 163
Wallace, L., & Hunten, D. M. 1973, ApJ, 182, 1013
Yung, Y. L., & Stroebel, D. F. 1980, ApJ, 239, 395

Online Material

Appendix A

The formalism of our problem is based on the 1-D radiative transfer equation considering the frequency redistribution. The one-dimensional, azimuthally averaged, non-linear integro-differential equation of radiative transfer can be written:

$$\mu \frac{\mathrm{d}I\left(z,\mu,x\right)}{\mathrm{d}z} + E\left(x,z\right) I\left(z,\mu,x\right) = E\left(x,z\right) S\left(z,\mu,x\right) \tag{3}$$

where:

$z \equiv$ height

$\mu \equiv$ cosine of the angle measured from vertical

$x \equiv$ frequency in Doppler units from the line centre

$I(z, \mu, x) \equiv$ specific intensity (photons cm^{-2} s^{-1} sr$^{-1}\Delta\nu_D^{-1}$)

$E(x, z) \equiv$ total extinction per unit path length which is defined by:

$$E\left(x,z\right) = n_{\mathrm{a}}\left(z\right)\sigma_{\mathrm{a}} + n_{\mathrm{s}}\left(z\right)\sigma_{\mathrm{s}}\left(z,x\right) \tag{4}$$

where "n" stands for densities in cm^{-3} and σ stands for cross section; the index "a" represents absorption while the index "s" represents scattering.

Assuming that the solar/external source has been separated from the diffused radiation, the source function is given by:

$$\begin{aligned} S\left(z,\mu,x\right) \;=\; & \frac{1}{E\left(x,z\right)} \frac{\varpi n_{\mathrm{s}}\left(z\right)}{2} \int_{-\infty}^{+\infty} \mathrm{d}x' \sigma_{\mathrm{s}}\left(z,x'\right) \int_{-1}^{+1} \mathrm{d}\mu' r\left(z,\mu,x,\mu',x'\right) I\left(z,\mu',x'\right) \\ & + \frac{1}{E\left(x,z\right)} \frac{\varpi n_{\mathrm{s}}\left(z\right)}{4\pi} \int_{-\infty}^{+\infty} \mathrm{d}x' \sigma_{\mathrm{s}}\left(z,x'\right) r\left(z,\mu,x,\mu_0',x'\right) \pi F\left(x\right) \exp\left(\tau\left(z,x'\right)\right) \frac{\varpi}{4\pi} \\ & + \frac{1}{E\left(x,z\right)} \varpi \frac{V\left(z,x\right)}{4\pi} \end{aligned} \tag{5}$$

where:

$\varpi \equiv$ single scattering albedo

$\mu_0 \equiv$ cosine of solar zenith angle

$r(z, \mu_0, x, \mu', x') \equiv$ frequency redistribution function

$\pi F(x) \equiv$ solar flux (photons cm^{-2} s^{-1})

$$\tau(z,x) = \int_{z}^{+\infty} \mathrm{d}z' E\left(z',x\right) \tag{6}$$

is the vertical optical depth;

$\frac{V(z,x)}{4\pi} \equiv$ total volume production rate of an isotropic internal source.

The scattering cross sections are computed from:

$$\sigma_{\mathrm{s}}\left(z,x\right) = \sigma_0\left(z\right)\phi\left(a\left(z\right),x\right) = \frac{\pi e^2 f}{m_{\mathrm{e}} c} \frac{\phi\left(a\left(z\right),x\right)}{\sqrt{\pi}\Delta\nu_{\mathrm{D}}\left(z\right)} \tag{7}$$

f is the oscillator strength.

$\Phi(a(z), x) \equiv$ Voigt profile, i.e. the convolution of a Gaussian profile (from Doppler width) and a Lorenztian profile (from natural line broadening).

$$\phi\left(a\left(z\right),x\right) = \frac{2a\left(z\right)}{\pi^3} \int_{-\infty}^{+\infty} \frac{\mathrm{e}^{-y^2}}{a\left(z\right)^2 + \left(x-y\right)^2} \mathrm{d}y \tag{8}$$

where "a" is the ratio between the Doppler width $\Delta\nu_{\mathrm{D}}(z)$ and the natural line width.

This transfer equation includes an isotropic scattering phase function with an arbitrary frequency redistribution and both external and internal sources.

The classical solving procedure uses the differential equation approach (Cannon 1985). The present integral equation approach first calculates the source function, $S(z, \mu, x)$. The conversion of Eq. (5) to an integral equation is desirable to facilitate the manipulation of this problem to generate physical solutions satisfying the equation, and is done as follows: rearrange Eq. (5) so as to leave $S(z, \mu, x)$ only on the right-handside. Then we can immediately write:

$$\frac{\mathrm{d}\left[I\mathrm{e}^{-\tau/\mu}\right]}{\mathrm{d}\tau\left(z,x\right)} = -\frac{\mathrm{e}^{-\tau(z,x)/\mu}}{\mu} S\left(z,\mu,x\right). \tag{9}$$

The upwelling radiation flux is defined by (Cannon 1985):

$$I^{+}(z,\mu,x) = \exp\left(-\left(\tau\left(z_{\min},x\right)-\tau\left(z,x\right)\right)/\mu\right) I^{+}\left(z_{\min},\mu,x\right) + \int_{z_{\min}}^{z} \mathrm{d}z' \frac{E\left(z',x\right)}{\mu} S\left(z',\mu,x\right) \left(\exp\left(-\left(\tau\left(z_{\min},x\right)-\tau\left(z,x\right)\right)/\mu\right)\right. . \tag{10}$$

The downwelling radiation flux is defined by

$$I^{-}(z,\mu,x) = \exp\left(-\left(\tau\left(z_{\min},x\right)-\tau\left(z,x\right)\right)/\mu\right) I^{-}\left(z_{\max},\mu,x\right) + \int_{z}^{z_{\max}} \mathrm{d}z' \frac{E\left(z',x\right)}{\mu} S\left(z',\mu,x\right) \left(\exp\left(-\left(\tau\left(z_{\min},x\right)-\tau\left(z,x\right)\right)/\mu\right)\right. \tag{11}$$

where $0 \leq \mu < 1$. For the majority of cases $I^{+}(z_{\min}, -\mu, x)$ and $I^{-}(z_{\max}, \mu, x)$ will be set to zero (i.e. zero diffuse incident radiation flux at the top of the atmosphere and no radiation flux downwelling at the bottom of the atmosphere). Incorporating this assumption, integral Eqs. (10) and (11) are now substituted into Eq. (3). This results in an integral equation in $S(z, \mu, x)$ only:

$$\begin{aligned} S\left(z,\mu,x\right) \;=\; & \frac{\varpi\left(z,x\right) n_{\mathrm{s}}\left(z\right)}{2E\left(z,x\right)} \int_{-\infty}^{+\infty} \mathrm{d}x' \sigma_{\mathrm{s}}\left(z,x'\right) \\ & \times \left[\int_{0}^{1} \mathrm{d}\mu' r\left(z,\mu,x,_{m}u',x'\right) \int_{z_{\min}}^{z} \mathrm{d}z' \frac{E\left(z',x'\right)}{\mu'} S\left(z',\mu',x'\right) .\mathrm{e}^{\left[-\left(\tau\left(z',x'\right)-\tau\left(z,x'\right)\right)/\mu'\right]} \right. \\ & \left. + \int_{0}^{+1} \mathrm{d}\mu' r\left(z,\mu,x,-\mu',x'\right) \int_{z_{\max}}^{z} \mathrm{d}z' \frac{E\left(z',x'\right)}{\mu'} S\left(z',-\mu',x'\right) .\mathrm{e}^{\left[-\left(\tau\left(z,x'\right)-\tau\left(z',x'\right)\right)/\mu'\right]} \right] + S_{0} \end{aligned} \tag{12}$$

where

$$S_{0} = \frac{1}{E\left(z,x\right)} \left[\frac{\varpi\left(z,x\right) n_{\mathrm{s}}\left(z\right)}{4\pi} \int_{-\infty}^{+\infty} \mathrm{d}x' \sigma_{\mathrm{s}}\left(z,x\right) R\left(z,x,\mu,x',-\mu_{0}\right) \pi F\left(x'\right) \frac{\varpi\left(z,x'\right)}{4\pi} \exp\left[\tau\left(z,x'\right)/\mu_{0}\right] + \varpi\left(z,x\right) \frac{V\left(z,x\right)}{4\pi} \right]. \tag{13}$$

The Feautrier technique has been described in detail previously (Mihalas 1978; Gladstone 1983; Cannon 1985; Griffoen 2000). The technique overcomes the exponential error increasing with optical depth by transforming the radiative transfer equation into second order integro-differential form. Expanding the two boundary conditions through the atmosphere, we constrain these errors.

Our most difficult problem is that of the overlapping of different lines, which has to be included in the formulation of this problem. To this purpose, we use a different formulation of the source term (Griffoen 2000; Parkinson 2002).

$$\begin{aligned} S\left(z,\mu,x\right) \;=\; & \frac{1}{E\left(z,x\right)} \frac{\varpi_{\mathrm{H}_2} n_{\mathrm{H}_2}\left(z\right)}{2} \int_{-\infty}^{+\infty} \mathrm{d}x' \sigma_{\mathrm{H}_2}\left(z,x'\right) \int_{-1}^{+1} \mathrm{d}\mu' r_{\mathrm{H}_2}\left(z,\mu,x,\mu',x'\right) I\left(z,\mu',x'\right) \\ & + \frac{1}{E\left(z,x\right)} \frac{\varpi_{\mathrm{H}} n_{\mathrm{H}}\left(z\right)}{2} \int_{-\infty}^{+\infty} \mathrm{d}x' \sigma_{\mathrm{H}}\left(z,x'\right) \int_{-1}^{+1} \mathrm{d}\mu' r_{\mathrm{H}}\left(z,\mu,x,\mu',x'\right) I\left(z,\mu',x'\right) \\ & + \frac{1}{E\left(z,x\right)} \frac{1}{4\pi} \int_{-\infty}^{+\infty} \mathrm{d}x' \left(\varpi_{\mathrm{H}_2} n_{\mathrm{H}_2}\left(z\right) \sigma_{\mathrm{H}_2}\left(z,x'\right) r_{\mathrm{H}_2}\left(z,\mu,x,-\mu_{0}',x'\right) + \varpi_{\mathrm{H}} n_{\mathrm{H}}\left(z\right) \sigma_{\mathrm{H}}\left(z,x'\right) r_{\mathrm{H}}\left(z,\mu,x,-\mu_{0}',x'\right) \right). \\ & \pi F\left(x'\right) \mathrm{e}^{\left[\tau\left(z,x'\right)/\mu_{0}\right]} \end{aligned} \tag{14}$$

where

$$E\left(z,x\right) = n_{\mathrm{H}}\left(z\right) \sigma_{\mathrm{H}}\left(z,x\right) + n_{\mathrm{H}_2}\left(z\right) \sigma_{\mathrm{H}_2}\left(z,x\right) + n_{\mathrm{CH}_4}\left(z\right) \sigma_{\mathrm{CH}_4}\left(z,x\right) \tag{15}$$

and

$$E\left(z,x\right) = N_{\mathrm{H}}\left(z\right) \sigma_{\mathrm{H}}\left(z,x\right) + N_{\mathrm{H}_2}\left(z\right) \sigma_{\mathrm{H}_2}\left(z,x\right) + N_{\mathrm{CH}_4}\left(z\right) \sigma_{\mathrm{CH}_4}\left(z,x\right) \tag{16}$$

N_i is the column amount of species i. Note that we have taken into account the absorption by CH_4, and since there is no resonant emission line of CH_4, we include CH_4 only in the absorption term.